Comptonization in the accretion column of the X-ray pulsar GX 1+4

D. K. Galloway[1]

School of Mathematics and Physics, University of Tasmania, Hobart, Australia 7001

RCfTA, University of Sydney, Camperdown, NSW 2006

Received _____; accepted _____

[1]present address: Center for Space Research, MIT, 77 Massachusetts Avenue, Cambridge, MA 02139-4307

ABSTRACT

X-ray observations of the binary pulsar GX 1+4 made using the Rossi X-ray Timing Explorer (*RXTE*) satellite between February 1996 and May 1997 were analysed to quantify source spectral variation with luminosity.

Mean Proportional Counter Array (PCA) spectra over the range 2–40 keV are best fitted with a Comptonization model, with source spectrum temperature $T_0 \approx$ 1–1.3 keV, plasma temperature $T_e \approx$ 6–10 keV, and optical depth $\tau \approx$ 2–6. The range of fitted T_0 was consistent with the source spectrum originating at the neutron star polar cap, with Compton scattering taking place primarily in the hot plasma of the accretion column. Both the fitted optical depth and plasma temperature vary significantly with the source flux. The variation of the optical depth (and hence the density of the scattering region) with luminosity strongly suggests increasing cross-sectional area of the accretion column at higher accretion rate $\dot{M}$.

The wide range of source luminosity spanned by archival observations of GX 1+4 offers evidence for two distinct spectral states above and below $L_X \approx 2 \times 10^{37}$ erg s^{-1} (2–60 keV, assuming a source distance of 10 kpc). GX 1+4 additionally exhibits dramatic hourly variations in neutral column density n_H indicative of density variations in the stellar wind from the giant companion.

Subject headings: X-rays: stars — pulsars: individual (GX 1+4) — accretion — scattering

1. Introduction

At the time of its discovery (Lewin et al. 1971) GX 1+4 was one of the brightest objects in the X-ray sky. The optical counterpart is an M6 giant (Davidsen et al. 1977) which is readily classified as a symbiotic binary (Belczynski et al. 2000). Unusually this LMXB appears to be accreting from the companions' stellar wind, which infrared observations suggest is at least an order of magnitude faster than typical red giant winds (Chakrabarty et al. 1998) and which presumably also gives rise to the optical emission line nebula. Optical spectroscopy suggests a source distance of 3–15 kpc (Chakrabarty & Roche 1997).

Measurements of the average spin-up rate during the 1970s gave the largest value recorded for any pulsar (or in fact any astronomical object) at ≈ 2 per cent per year. Inexplicably, the average spin-up trend reversed around 1983, switching to spin-down at approximately the same rate. Since that reversal a number of changes in the sign of the torque (as inferred from the rate of change of the pulsar spin period) have been observed (Chakrabarty et al. 1997). In contrast to predictions of the Ghosh & Lamb (1979a,b) model BATSE measurements suggest that the torque measured for GX 1+4 is sometimes *anticorrelated* with luminosity (Chakrabarty et al. 1997). This behaviour has not been observed in other pulsars. The orbital period is not known, but secular torque variations suggest $P_{\rm orb} \approx 304$ d (Cutler et al. 1986; Pereira et al. 1999). Several estimates (Beurle et al. 1984; Dotani et al. 1989; Mony et al. 1991; Greenhill et al. 1993; Cui 1997) indicate a neutron star surface magnetic field strength of $2–3\times10^{13}$ G.

The X-ray flux from the source is extremely variable on time-scales of seconds to decades. Two principal flux states have been suggested, a 'high' state which persisted during the spin-up interval of the 1970s, and a 'low' state since. Superimposed on the long-term flux variations are smooth changes on time-scales of order hours to days. On the shortest time-scales the periodic variation due to the neutron star's rotation period

at around 2 min is observed. Pulse profiles from the source exhibit a bewildering variety of shapes. The profiles are typically asymmetric, with a sharp dip forming the primary minimum (Dotani et al. 1989; Greenhill et al. 1998; Kotani et al. 1999, , Galloway & Greenhill 2000, in preparation). These dips appear to be signatures of near-field 'eclipses' of the polar cap by the accretion stream (Galloway et al. 2000, in preparation). The sense of asymmetry of the profiles is variable on timescales as short as a few hours (Giles et al. 2000).

Historically the X-ray spectrum has been fitted with bremsstrahlung or power law models, however more recent observations with improved spectral resolution generally favour a power law model with exponential cutoff. In general the various power-law models are an approximation to a spectrum originating from a low-energy distribution of photons Comptonized by scattering within a hotter plasma (e.g. Pozdnyakov et al. 1983). The accretion column plasma reaches the highest density immediately above the polar cap, where the X-ray photons are thought to be emitted. Compton scattering in the accretion column is likely to be an important process affecting the initial photon spectrum. More detailed approximations to Comptonized spectra are an obvious choice for candidate X-ray pulsar models; the Titarchuk (1994) formulation has previously been used in fits to *RXTE* spectra (Galloway et al. 2000). For any spectral model covering the range 1-10 keV, it is also necessary to include a gaussian component representing iron line emission at ≈ 6.4 keV, and a term to account for the effects of photoelectric absorption by cold gas along the line of sight with hydrogen column density in the range $n_H = (4 - 140) \times 10^{22}$ cm^{-2}. The source spectrum and in particular the column density n_H have previously exhibited significant variability on time-scales of a day or less (Becker et al. 1976; Galloway et al. 2000).

The public archival data now available from *RXTE* observations of the source has allowed a test of the applicability of Comptonization models to spectra over a wide range

of source luminosities.

2. Observations

RXTE consists of three instruments, the proportional counter array (PCA) sensitive to photons in the energy range 2–60 keV, the high-energy X-ray timing experiment (HEXTE) covering 16–250 keV, and the all-sky monitor (ASM) which spans 2–10 keV (Giles et al. 1995). Pointed observations are performed using the PCA and HEXTE instruments, while the ASM regularly scans the entire visible sky. During targeted observations, interruptions may be made for previously scheduled monitoring or target-of-opportunity (TOO) observations of other sources.

Six of the eight event analysers (EAs) aboard *RXTE* are available for processing of events measured by the PCA. Two EAs are dedicated to modes which are always present, 'Standard-1' and 'Standard-2'. The Standard-1 mode features 0.25 μs time resolution but only one spectral channel, while Standard-2 offers 129 spectral channels between 0–100 keV (the sensitivity above 60 keV is negligible) with binning on 16 s time resolution. The remaining four EAs may be used in a range of user-configurable modes, which are in general only necessary to obtain spectra on a finer time resolution.

Between February 1996 and May 1997 GX 1+4 was observed by *RXTE* in 25 distinct intervals totalling $\approx$ 230 ks (Table 1). From mid-1996 onwards two of the five proportional counter units (PCUs) which make up the PCA were intermittently turned off to partially arrest a gradual sensitivity degradation measured by the *RXTE* team. All 5 PCUs were on for the majority of the observations. PCUs 3 and 4 were commanded off during observations D, N and P, and for part of observation H. PCU 4 alone was off for short intervals during observations H and R. The countrate for these observations was scaled appropriately to

give the equivalent for all 5 PCUs on. The phase-averaged countrate from the source demonstrates its dramatic variability (Figure 1). The pulse period for the averaging has been determined by phase folding or interpolation of BATSE period measurements; see Galloway & Greenhill 2000, in preparation. The countrate can span more than two orders of magnitude in less than two days (e.g. observation H; Giles et al. 2000). More typically the countrate varies by a factor of ~ 5 on hourly timescales when the countrate was 100 ct s^{-1} or more, and a factor of ~ 10 otherwise. Increased variability at low flux levels was also noted by Greenhill et al. (1999) in analyses of archival hard X-ray observations. These variations were superimposed on long-term trends with timescales of a year or more, which may be related to the orbital period (Pereira et al. 1999). The source appeared to be relatively bright during the first half of 1996, after which it entered a ≈ 50 d low state. The decrease in 20–60 keV flux was much more abrupt than the PCA countrate. At this time pulsations from the source all but ceased, suggesting cessation of mass transfer from the companion or possibly centrifugal inhibition of accretion (Cui 1997). A flare lasting about 30 days was observed by BATSE during August 1996, following the period of lowest flux during July. After the flare the source returned to a relatively low state, which persisted to June 1997. The PCA countrate generally traces the 20–60 keV flux as measured by BATSE reasonably well, but spectral variation in the source (in particular the degree of low-energy absorption) means that the contribution from high-energy photons varies.

3. Spectral analysis

Analysis of Standard-2 *RXTE* data presented in this paper was carried out using LHEASOFT 5.0, released 23 February 2000 by the *RXTE* Guest Observer Facility (GOF). The data were first screened to ensure that the pointing offset was $< 0.02°$ and the source was $> 10°$ from the sun. This introduces additional gaps to the data. If individual PCUs

are switched off or on during the observation it was necessary to extract spectra from each interval with a constant number of PCU's on and analyse them separately. Observations were subdivided when significant countrate variations are seen within the observation (e.g. observations A and H). As the spectral fit parameters (particularly the column density $n_{\rm H}$) tend to vary on hourly timescales it may be necessary to further subdivide intervals to obtain adequate fits. Subintervals were labeled with the appropriate letter from Table 1 and a number (e.g. A1, A2 ...). Example spectra are shown in Figure 2.

Instrumental background from cosmic ray interactions and as a result of satellite passages close to the SAA were estimated using the PCABACKEST software which is included in the LHEASOFT package. The background models used were also from the 23 February 2000 release. Where the net source countrate was $\lesssim 60\,{\rm count\,s^{-1}}$ the 'faint' source models have been used, with the 'bright' models used otherwise.

Candidate spectral models were tested by fitting to the count rate spectrum to minimise the reduced-χ^2 ($= \chi^2_\nu$) using the XSPEC spectral fitting package version 11 (Arnaud 1996). XSPEC allows spectral fitting given some assumed level of *systematic* error in the instrumental calibration, which clearly will affect the fit statistic. However no systematic error was assumed in the spectral fits undertaken in this paper. In general each model takes the form of at least one continuum component and a multiplicative component to account for absorption by cold matter along the line of sight. Continuum components tested for the GX 1+4 spectra include powerlaw, broken powerlaw, powerlaw and blackbody and powerlaw with exponential cutoff, as well as the Titarchuk (1994) Comptonization approximation implemented in XSPEC as '`compTT`'. Parameters for the latter component include the input spectrum temperature T_0 (approximated as a Wien law), the scattering plasma temperature $T_{\rm e}$ and normalisation $A_{\rm C}$ (in units of photons $\rm cm^{-2}\,s^{-1}\,keV^{-1}$). Additionally the redshift can be specified, but this was fixed at 0.0 for the model fits

described in this paper. The effective optical depth τ is calculated from the spectrum assuming either a spherical or planar (disc) geometry. If the accretion column *is* the primary region where Compton scattering takes place, clearly neither of these assumptions are strictly appropriate. For the `compTT` model fits presented in this paper I adopt the 'disc' geometry switch, noting that the calculated τ will thus be only an approximate measure of the true optical depth in the column. In general the calculated τ for an assumed spherical geometry will be approximately twice as large.

A gaussian component with energy ≈ 6.4 keV simulates the (generally) significant iron line emission. Due to its proximity to the galactic plane, an additional component which takes into account the so-called 'galactic ridge' emission must also be included in the spectral model. This component is modelled using a Raymond-Smith emission spectrum from hot, diffuse gas and a powerlaw, both absorbed by a neutral column density of $n_{\rm H} = 2 \times 10^{21}\,{\rm cm}^{-2}$. Two additional power law components serve as a correction to the diffuse X-ray background assumed by PCABACKEST. The model was identical to that fitted to survey data from this region Valinia & Marshall (1998) with normalisations and metal abundance as fitted to spectra taken during slews to and from the source in July 1996 (observation H in Table 1; Galloway et al. 2000). A final instrumental effect which must be taken into account to obtain the lowest possible residuals in the model fit is a consequence of the Xenon L-edge absorption feature. This feature is modelled by a multiplicative edge model component with energy fixed ('frozen') at 4.83 keV.

4. Results

For any spectral model, the fit statistic χ^2_ν depends strongly on the countrate during the observation. When the countrate (and hence the source-to-background ratio) is low, errorbars on the spectral bins will be large, and typically more than one (if not all) of the

models will give a statistically acceptable spectral fit. The comparison between the models for those observations at the highest available countrates (e.g. A...E, Q...U) provides a much more stringent test. For the powerlaw continuum during these intervals χ^2_ν varies from $\approx$ 2–150, typically ≈ 5. A powerlaw modified by an exponential high-energy cutoff provides some improvement, with typical values $\approx$ 1.5–6, as does a broken power law (with two spectral indexes above and below some 'break' energy) giving $\chi^2_\nu \approx$ 1.5–4. A combination powerlaw and blackbody was acceptable for most of the observations with typical values ≈ 1.3, but can be as high as e.g. $\chi^2_\nu \approx 25$ for observation A1. Only the Comptonization continuum gives $\chi^2_\nu \lesssim 2.5$ for each of the spectra tested.

The correlation between χ^2_ν for the Comptonization component fits and the integrated source flux is readily apparent although there is also significant scatter about the line of fit (Figure 3). Significant variations in χ^2_ν were seen even between immediately adjacent observations (e.g. R1/R2/R3). While it was necessary to subdivide certain intervals (most noticeably the second half of observation A) to obtain reasonable values of χ^2_ν, the Comptonization model still unambiguously offers the best fit over the shorter integration times resulting. The spectrum extracted from observation Y2 is a rather special case; see Galloway 2000, in preparation.

The fitted values of the source spectrum temperature T_0 were seen to cluster strongly around the weighted mean of 1.284 ± 0.004 keV (1σ) over a wide range of flux (Figure 4a). Below $\approx 3 \times 10^{36}$ erg s^{-1} the fit values were subject to large uncertainties but were broadly consistent with $T_0 \lesssim 3$ keV. The fit parameter ranges are limited at the lower boundary by the minimum allowed by the `compTT` implementation in XSPEC of 0.001. Several spectra suggest $T_0 < 1$ keV, however the 90 per cent error limits were large and these may not be significant.

The fitted optical depth τ varies between 2–6 over the flux range of 10^{36}–10^{38} erg s^{-1}

(Figure 4b). This figure omits the value for observation Y2, which was by far the highest measured at around $\tau = 19.4^{21.1}_{18.3}$. When the flux was $\lesssim 2 \times 10^{37}$ erg s^{-1} the τ values cluster around 3, whereas above that a range of 4-6 is more typical. The corresponding mean values were 2.95 ± 0.47, and 4.7 ± 1.0 respectively, which disagree at the 1.6σ level. The variance was substantially greater at high flux. The observed variation may be viewed as a rough correlation between τ and $L_{\rm X}$. To test the significance of the relationship I use the BCES(Y—X) estimator of Akritas & Bershady (1996). Ordinary weighted least squares methods are not strictly appropriate for fitting data with heteroscedastic (varying) errors in both parameters, and where there are thought to be *systematic* errors in addition to measurement errors in the parameters. The resulting gradient for a linear fit confirms a significant relationship, with gradient $b = 0.450 \pm 0.070$. However, separate linear fits to the data above and below $L_{\rm X} = 2 \times 10^{37}$ erg s^{-1} tell a different story, with gradients $b = -0.0354 \pm 0.638, -1.41 \pm 1.01$ respectively.

It is possible that the variation of fitted τ values is due to aliasing by some dependence of the fitting algorithm on the varying countrate. This can be tested by (for example) selecting a spectral model with parameters from one of the higher flux observations, generating a simulated spectra with much lower flux, and comparing the resulting spectral fitting results. In general the spectral parameters were found to depend only weakly on flux for simulated observations. There was certainly no abrupt drop to lower τ values as the simulated flux was decreased. Visual inspection of representative spectra from the high- and low-τ groups further supports the significant differences between the two (Figure 2). Fits to mean spectra from observations B and E give consistent column densities $n_{\rm H} = 5.51^{5.66}_{5.36}$ and $5.37^{5.72}_{5.00}$ respectively. However, the peak in the spectra clearly occurs at different energies. The PHA ratio between the two demonstrates that the high-energy slopes are different, as is the turnover energy (where the slope changes around 10 keV; note the 'kink' in the PHA ratio around that energy).

The corresponding plot for T_e also shows evidence for a non-isotropic distribution of the points, but to a lesser extent (Figure 4c). The points appear to fall into two groups again roughly divided at a flux level of $\approx 2 \times 10^{37}$ erg s^{-1}. Above this level $T_e \lesssim 10$ keV typically, whereas below T_e values were generally higher although with very large errorbars. The distribution may be viewed as an anticorrelation of T_e with flux; the resulting BCES(Y—X) slope was -1.76 ± 0.54. Within the two groups T_e appears to increase with flux, although no significant linear relationship was found. With low countrates it was much more difficult to determine T_e precisely, and in fact for approximately half the spectra which fall into this lower flux range the value cannot be determined at all (note the smaller number of points in Figure 4c compared to a,b). For these spectra I fix the value at 10 keV, consistent with the mean for the group 10.6 ± 2.1. This was different from the mean for the higher flux group, 7.8 ± 1.2, at low signifcance only ($\approx 1.2\sigma$).

The Compton y-parameter can be calculated for each spectra from the fitted τ, T_e. Since $kT_e \ll m_e c^2$ the nonrelativistic form is more appropriate (Rybicki & Lightman 1979). The plot of y as a function of source flux exhibits similar clustering to the corresponding plots with τ, T_e (Figure 4d). The two groups fall neatly on either side of the line $y = 1$, normally considered the limiting value between spectra which are weakly modified ($y \ll 1$) and spectra strongly modified ($y \gg 1$) by Comptonization.

The absorption column density n_H varies by more than two orders of magnitude over the course of the observations, often on timescales as short as a few hours (e.g. observations A and H). This parameter is roughly correlated with the iron line equivalent width (Figure 5a). At lower n_H the EW was also generally lower, but the results from 11-21 July 1996 (G,H) populate a distinctly different area of the graph than the majority of spectra, with EW$\lesssim 300$ but n_H well above 10^{23} cm^{-2}. Also dramatically different was the point for observation Y2, with $n_H \approx 10^{23}$ cm^{-2} but EW≈ 1.8 keV. Trajectories traced out in n_H–EW

space as the spectra evolve with time tend to move diagonally, following the mean slope of the correlation, but there were also significant excursions at various other angles. The line energy itself appears to be roughly correlated with T_e (Figure 5b). This does not seem to be a consequence of a correlation with flux instead, since spectra with widely different values of flux frequently appear to fall on similar regions of the graph.

5. Discussion

The archival data accumulated through *RXTE* observations of GX 1+4 cover a wide range of source conditions for this enigmatic pulsar. Particularly clear is the degree of variability of the source on all timescales, from seconds to years.

Analysis of the previously unpublished observations have provided some important new results. During February 1996 the source was close to the brightest level seen by *RXTE* between 1996 and mid-1997, and the $\approx$ 1 d observation at that time featured a dramatic rise in scattering column density n_H over just a few hours. This event was very similar to that observed during July 1996 (observation H; Galloway et al. 2000). Such events are clearly quite common and this strongly suggests n_H variations are a significant source of observed countrate modulation on hourly (and longer) timescales. The modest collecting area of *RXTE* does not provide a high enough countrate to resolve spectral variations on smaller timescales, but n_H variations may have a significant influence there too.

The iron line energy and the relationship between equivalent width and n_H were roughly consistent with the spherical distribution of matter inferred by Kotani et al. (1999). However the minimum timescale of n_H variations $\approx$ 2 h is much too rapid to be attributable to the negative feedback effect which those authors suggest regulates mass transfer to the neutron star in the long term. The variation may instead be an indication of significant

inhomogeneities in the stellar wind from the companion on spatial scales of

$$\delta s \sim 7 \times 10^9 \left(\frac{v_{\rm w}}{10 \ {\rm km\,s^{-1}}} \right) \ {\rm cm} \tag{1}$$

along the line of sight to the neutron star. Infrared observations suggest that $v_{\rm w}$ may be as much as 250 $\rm km\,s^{-1}$ (Chakrabarty et al. 1998), but since the line of sight may intercept the system at varying distances form the companion (depending upon the orbital phase) the local wind speed may also vary due to deceleration. The rough correlation between $E_{\rm Fe}$ and $T_{\rm e}$ suggests that there is also a contribution to the Fe line emission from the accretion column. The relationship between τ and $T_{\rm e}$ shows that when the column plasma is cooler it also tends to be more optically thick; in which case the line emission from the column plasma will suffer greater self-absorption. Line emission will thus be dominated by the cool circumstellar matter, and the resulting line energy is indicative of very low ionisation levels. At lower source luminosities the column plasma becomes hotter and slightly more transparent, which makes the contribution by the more highly ionised column plasma more significant and increases the fit energy of the gaussian line component. This suggests that at low luminosities pulse phase dependence of the iron line spectral parameters may be observed. Certainly at high luminosities there are suggestions of phase dependence of e.g. the gaussian component normalisation (Galloway et al. 2000, in preparation).

The inclusion of all the archival *RXTE* data in the spectral analysis has confirmed the general applicability of the Comptonization model of Titarchuk (1994) to GX 1+4 spectra. Additionally, model fitting for spectra taken during high-$L_{\rm X}$ intervals excludes each of the alternative models tested to a high level of statistical significance. To assess the reliability of the Comptonization model component over the range of parameters obtained for GX 1+4, I calculate the β-parameter appropriate for disc geometries:

$$\beta = \frac{\pi^2}{12(\tau + 2/3)^2}(1 - e^{-1.35\tau}) + 0.45 e^{-3.7\tau} \ln \left(\frac{10}{3\tau} \right) \tag{2}$$

(Hua & Titarchuk 1995). For the range of τ and $T_{\rm e}$ appropriate for GX 1+4, the analytic

model has been shown to yield results consistent with Monte-Carlo simulations (Figure 6; Hua & Titarchuk 1995) and thus should provide reasonable results. The model simulates Comptonization in an unmagnetised plasma, and since the available evidence points towards a strong magnetic field in GX 1+4 (although this awaits confirmation by more direct measurements such as a cyclotron resonance line) the model fit parameters may not be an accurate measure of the source conditions. It is likely that the principal effect of the magnetic field will be to make the spectral parameters dependent on the emission angle. Hence the model fit parameters obtained from the mean spectra are expected to be an approximate measure of the actual physical conditions in the source (L. Titarchuk 1998, private communication).

The source spectrum presumably originates from the polar cap itself, or perhaps a slab-shaped post-shock region of the column. Assuming that the majority of the X-ray emission originates from a blackbody at most the size of the neutron star ($R_* \approx 10$ km) the blackbody temperature is $T_0 \gtrsim 0.5$ keV. The model fit values for the input spectrum temperature $T_0 \approx 1.3$ keV was consistent with this calculation. The fit values for T_0 were remarkably consistent for the majority of spectra. The observation of a much lower value during observation A was the exception but the errors were quite large. (It is possible the latter measurements were related to a 'transitional' spectrum similar to that from observation Y2). The polar cap temperature is presumably maintained by the supply of energy from residual thermal and kinetic motion of the accreting plasma in competition with cooling by radiation and conduction through the neutron star crust. That the temperature varies little over the range of source luminosities points to extremely efficient cooling mechanisms.

Rough estimates of the accretion column density can be made based on the mass transfer rate derived from the luminosity, and assuming a simple column geometry. The

accretion luminosity $L_{\rm acc} \approx GM_*\dot{M}/R_*$ and thus

$$\begin{aligned} \dot{M} &\approx \frac{R_*}{GM_*} L_{\rm acc} \\ &= 5.0 \times 10^{16}\, L_{37}\ {\rm g\,s^{-1}} \end{aligned} \tag{3}$$

where $L_{\rm acc} = L_{37} \times 10^{37}\ {\rm erg\,s^{-1}}$. Assuming that the accretion column is homogeneous and cylindrical with radius $R_{\rm C} = fR_*$, and the column plasma is moving with constant velocity v (roughly equal to the free fall velocity $\approx 0.5c$), the estimated optical depth for Thompson scattering is

$$\begin{aligned} \tau &= R_{\rm C}\sigma_{\rm T} N_{\rm e} \\ &= \frac{2\dot{M}\sigma_{\rm T}}{\pi m_{\rm p} f R_* c} \\ &= 2.2\, L_{37} \left(\frac{f}{0.04}\right)^{-1} \left(\frac{v}{c}\right)^{-1} \end{aligned} \tag{4}$$

where $m_{\rm p}$ is the proton mass. In general f is subject to considerable uncertainties (e.g. Frank et al. 1992), and will depend on the inner disc radius since that defines which magnetic field lines form the edge of the accretion column at the neutron star surface. It is usually thought that $f = 0.01$–0.1, with smaller values appropriate for higher magnetic field systems (where the disc is disrupted further out from the neutron star on average). Regardless of the actual values, for the *RXTE* archival data with $L_{37} \in (0.1, 10)$ *constant* f implies that τ will also vary by around 2 orders of magnitude. The observed range of τ was dramatically different (Figure 4b) and thus it is clear that there are significant changes in accretion column structure as $L_{\rm X}$ varies.

The small range in τ (despite the two order-of-magnitude variation in $L_{\rm X}$) points to a partial regulation of the column density, possible through the following mechanism. As the accretion rate (and hence the luminosity) increases, the ram pressure from the gas in the accretion disc causes the accreting matter to thread magnetic field lines with footpoints at progressively lower (magnetic) latitudes on the star. The extent of the accretion column (f)

will increase, offsetting the density increase due to higher $\dot{M}$. As the luminosity increases, the effect of radiation pressure will also increase. As pointed out by Langer & Rappaport (1982), the effect of radiation pressure depends strongly on the isotropy of the radiation, since photons propagating at right angles to the magnetic field cannot affect the momentum of the plasma flow which is restricted to the local field direction. Nevertheless, an increased radiation pressure would reduce the flow velocity, increasing the density of the flow and hence the optical depth for scattering. From these arguments it seems much more likely that f was changing significantly as the accretion rate varied, and the contribution of radiation pressure was less important. This implies that over the observed flux range for the *RXTE* data f must vary by a factor of $\approx$ 30–50 in order to give the observed variation in τ.

Both τ and $T_{\rm e}$ appear to be roughly correlated with $L_{\rm X}$, the latter inversely. This correlation may partially arise from grouping of the fit values around significantly different means above and below $L_{\rm X} \approx 2 \times 10^{37}$ erg s^{-1}, since the correlation does not seem to be present in the high- or low-flux observations fitted separately. As discussed previously, this suggests two distinct spectral states for the source, although the physical differences between the two states are not clear. The combined variation of τ and $T_{\rm e}$ result in the calculated Compton y-values forming two groups which are separated by the line $y = 1$ (although the uncertainty was generally rather large). It should be noted that there was significant overlap in flux between the two groups, even neglecting the uncertainties which were also present in the flux estimations. This provides further evidence that some additional factor may give rise to the observed variation. It is compelling to suggest that the switch is due to a change from a situation when Comptonization is relatively unimportant to one where it is the dominant effect in spectral formation, but such distinctions are really only appropriate for the asymptotic cases $y \ll 1$ and $y \gg 1$ respectively. Additionally there is no way to estimate the systematic errors on any of the parameters involved, and so the fact that the y-values cross the $y = 1$ line as $L_{\rm X}$ increases was perhaps merely a coincidence. Nevertheless, the

jump may indeed be due to a switch to a significantly different accretion column structure. One possibility is that the accretion column becomes much less homogeneous. As the accretion rate increases, threading of the accreting plasma will become less efficient. Above $L_{\rm X} \approx 2 \times 10^{37}$ erg s^{-1} large blobs of relatively dense plasma may survive the accretion process without becoming threaded by magnetic field lines and thus dispersed, resulting in a significantly inhomogeneous column which may contribute to the greater scatter in τ at high $L_{\rm X}$. This inhomogeneity may introduce quasiperiodic oscillations similar to those observed in Cen X-3 (Jernigan et al. 2000). A search for such oscillations in GX 1+4 at varying mean flux levels would be a powerful test of this hypothesis.

The $T_{\rm e}$ parameter can be interpreted as a measure of the temperature of the accretion column plasma. However, the kinetic energy of the plasma from the infall velocity may be many orders of magnitude larger than the thermal energy. Photons undergoing Compton scattering in a plasma moving relative to the source will be scattered preferentially in the direction of motion, and the influence of the plasma temperature in its rest frame for the final photon distribution may be small. Thus the fitted value of $T_{\rm e}$ may owe more to the bulk plasma velocity than its temperature. With the significant uncertainties in the fit values it is difficult to make any qualitative statements about the variation with $L_{\rm X}$, but a net decrease in $T_{\rm e}$ with increasing $L_{\rm X}$ was the most robust result, possibly related to similar grouping of values as was observed with the τ values. The model normalisation parameter $A_{\rm C}$ is somewhat more difficult to relate to a physically measurable quantity, since both the $T_{\rm e}$ and τ parameters can also affect the total flux from the model component. Clearly in the absence of spectral variation it will generally be proportional to the source flux.

This research has made use of data obtained through the High Energy Astrophysics Science Archive Research Center Online Service, provided by the NASA/Goddard Space Flight Center, and also the BATSE Pulsar Group WWW

page at http://www.batse.msfc.nasa.gov/batse/pulsar. The *RXTE* Guest Observer Facility provided timely and vital help and information throughout.

REFERENCES

Akritas, M. G. & Bershady, M. A. 1996, ApJ, 470, 706

Arnaud, K. A. 1996, in ASP Conf. Ser. 101: Astronomical Data Analysis Software and Systems V, 17–20

Becker, R. H., Boldt, E. A., Holt, S. S., Pravdo, S. H., Rothschild, R. E., Serlemitsos, P. J., & Swank, J. H. 1976, ApJ, 207, L167

Belczynski, K., Mikolajewska, J., Munari, U., Ivison, R., & Friedjung, M. 2000, A&AS preprint

Beurle, K., Bewick, A., Harper, P., Quenby, J., Spooner, N., Fenton, A., Fenton, K., Giles, A., Greenhill, J., & Warren, D. 1984, AdSpR, 3(10–12), 43

Chakrabarty, D., Bildsten, L., Finger, M. H., Grunsfeld, J. M., Koh, D. T., Nelson, R. W., Prince, T. A., Vaughan, B. A., & Wilson, R. B. 1997, ApJ, 481, L101

Chakrabarty, D. & Roche, P. 1997, ApJ, 489, 254

Chakrabarty, D., van Kerkwijk, M. H., & Larkin, J. E. 1998, ApJ, 497, L39

Cui, W. 1997, ApJ, 482, L163

Cutler, E. P., Dennis, B. R., & Dolan, J. F. 1986, ApJ, 300, 551

Davidsen, A., Malina, R., & Bowyer, S. 1977, ApJ, 211, 866

Dotani, T., Kii, T., Nagase, F., Makishima, K., Ohashi, T., Sakao, T., Koyama, K., & Tuohy, I. R. 1989, PASJ, 41, 427

Frank, J., King, A. R., & Raine, D. J. 1992, Accretion power in astrophysics, 2nd edn. (Cambridge, England; New York, NY, USA: Cambridge University Press), 294

Galloway, D. K., Giles, A. B., Greenhill, J. G., & Storey, M. C. 2000, MNRAS, 311, 755

Ghosh, P. & Lamb, F. K. 1979a, ApJ, 232, 259

—. 1979b, ApJ, 234, 296

Giles, A., Galloway, D., Greenhill, J., Storey, M., & Wilson, C. 2000, ApJ, 529, 447

Giles, A. B., Jahoda, K., Swank, J. H., & Zhang, W. 1995, PASA, 12, 219

Greenhill, J. G., Galloway, D., & Storey, M. C. 1998, PASA, 15, 254

Greenhill, J. G., Galloway, D. K., & Murray, J. R. 1999, PASA, 16, 240

Greenhill, J. G., Sharma, D. P., Dieters, S. W. B., Sood, R. K., Waldron, L., & Storey, M. C. 1993, MNRAS, 260, 21

Hua, X.-M. & Titarchuk, L. 1995, ApJ, 449, 188

Jernigan, J. G., Klein, R. I., & Arons, J. 2000, ApJ, 530, 875

Kotani, T., Dotani, T., Nagase, F., Greenhill, J. G., Pravdo, S. H., & Angelini, L. 1999, ApJ, 510, 369

Langer, S. H. & Rappaport, S. 1982, ApJ, 257, 733

Lewin, W. H. G., Ricker, G. R., & McClintock, J. E. 1971, ApJ, 169, L17

Mony, B., Kendziorra, E., Maisack, M., Staubert, R., Englhauser, J., Dobereiner, S., Pietsch, W., Reppin, C., Trumpler, J., Churazov, E. M., Gilfanov, M. R., & Sunyaev, R. 1991, A&A, 247, 405

Pereira, M. G., Braga, J., & Jablonski, F. 1999, ApJ, 526, L105

Pozdnyakov, L. A., Sobel, I. M., & Syunyaev, R. A. 1983, Astrophysics and Space Physics Research, 2, 189

Rybicki, G. & Lightman, A. 1979, Radiative processes in astrophysics (New York: John Wiley & Sons), 382

Titarchuk, L. 1994, ApJ, 434, 570

Valinia, A. & Marshall, F. E. 1998, ApJ, 505, 134

This manuscript was prepared with the AAS LaTeX macros v5.0.

Table 1. *RXTE* observations of GX 1+4. Start and end times and on-source durations are calculated from Standard-2 spectra taking into account screening. Times are terrestrial time (TT).

ID	Start	End	On-source (sec)	Ref.
A	12/02/1996 14:11:11	13/02/1996 13:35:11	46816	
B	17/02/1996 03:12:15	17/02/1996 08:12:02	10400	[1]
C	23/04/1996 19:10:23	23/04/1996 22:40:15	7680	[1]
D	21/05/1996 15:45:03	21/05/1996 18:08:15	5568	[1]
E	08/06/1996 04:49:14	08/06/1996 11:58:34	10112	[1]
F	28/06/1996 06:41:03	28/06/1996 23:35:35	5392	[1]
G	11/07/1996 18:23:27	11/07/1996 22:08:40	3552	[1]
H	19/07/1996 16:47:16	21/07/1996 02:39:02	52832	[2,3]
I	04/09/1996 22:33:35	05/09/1996 03:05:00	9232	[1]
J	25/09/1996 11:12:15	25/09/1996 15:19:04	6672	[1]
K	08/10/1996 09:43:32	08/10/1996 10;38:44	3280	[1]
L	16/10/1996 18:32:38	16/10/1996 23:07:11	6016	[1]
M	24/10/1996 17:58:39	24/10/1996 19:51:27	4528	[1]
N	01/11/1996 03:35:27	01/11/1996 05:34:02	4720	[1]
O	07/11/1996 18:26:00	07/11/1996 20:23:59	4592	[1]
P	10/11/1996 12:16:16	10/11/1996 14:13:02	4688	[1]
Q	16/01/1997 00:27:11	16/01/1997 02:24:03	4592	[1]
R	16/01/1997 03:16:35	16/01/1997 08:02:04	9760	
S	21/01/1997 19:13:51	21/01/1997 21:32:31	5152	[1]
T	26/01/1997 22:57:03	27/01/1997 00:54:15	4672	[1]
U	02/02/1997 14:35:11	02/02/1997 16:50:02	4512	[1]
V	26/02/1997 00:41:15	27/02/1997 18:48:31	2816	
W	20/03/1997 16:39:00	25/03/1997 18:56:02	4768	
X	18/04/1997 12:34:28	22/04/1997 23:45:02	4592	
Y	16/05/1997 03:35:27	20/05/1997 07:04:36	4080	

References. — [1] Cui (1997); [2] Galloway et al. (2000); [3] Giles et al. (2000)

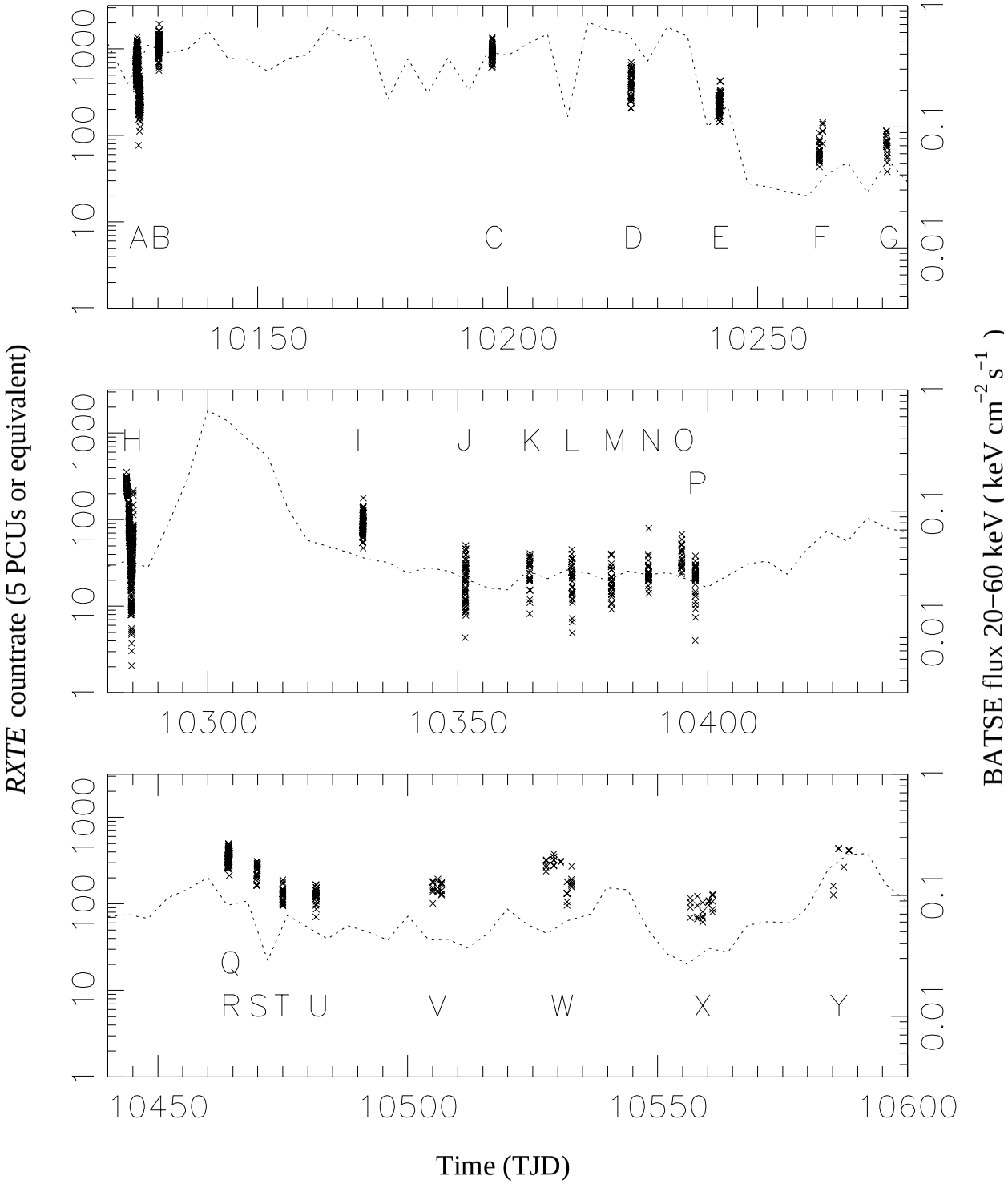

Fig. 1.— *RXTE* and BATSE observations of GX 1+4 between Feburary 1996 and May 1997. Phase-averaged background-subtracted countrate from pointed observations using the PCA aboard *RXTE* are plotted as crosses (left hand scale in each panel). The observations are labelled A...Y; see Table 1. The dotted line represents the 20–60 keV pulsed flux as measured by BATSE (right hand scale).

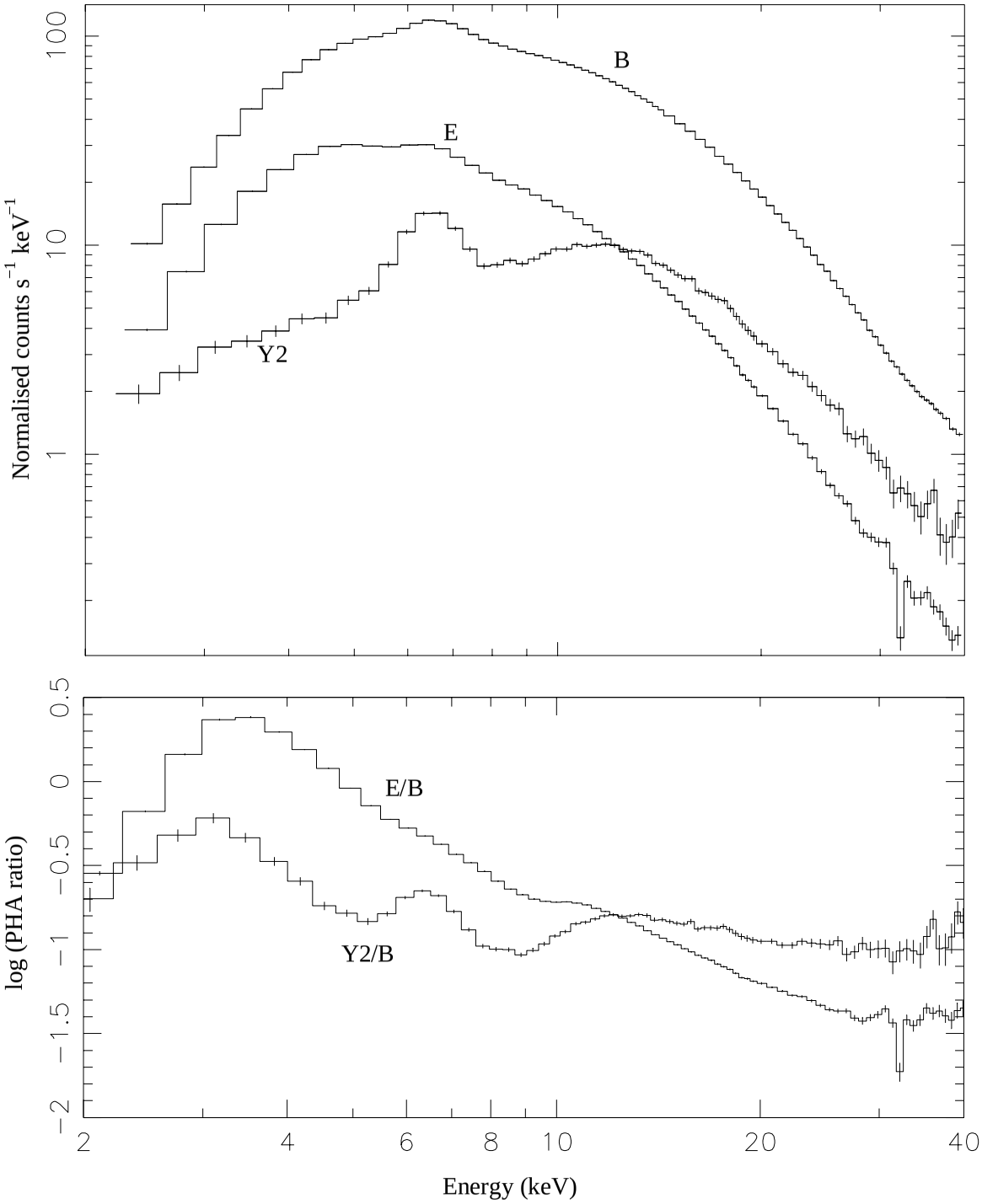

Fig. 2.— Sample raw *RXTE* spectra from GX 1+4. The top panel plots mean spectra from observations B (17 February 1996), E (8 June 1996) and Y2 (17 May 1997). The bottom panel shows the PHA ratio calculated by dividing the countrate in each spectral bin for spectra from observations E and Y2 by the spectrum from observation B.

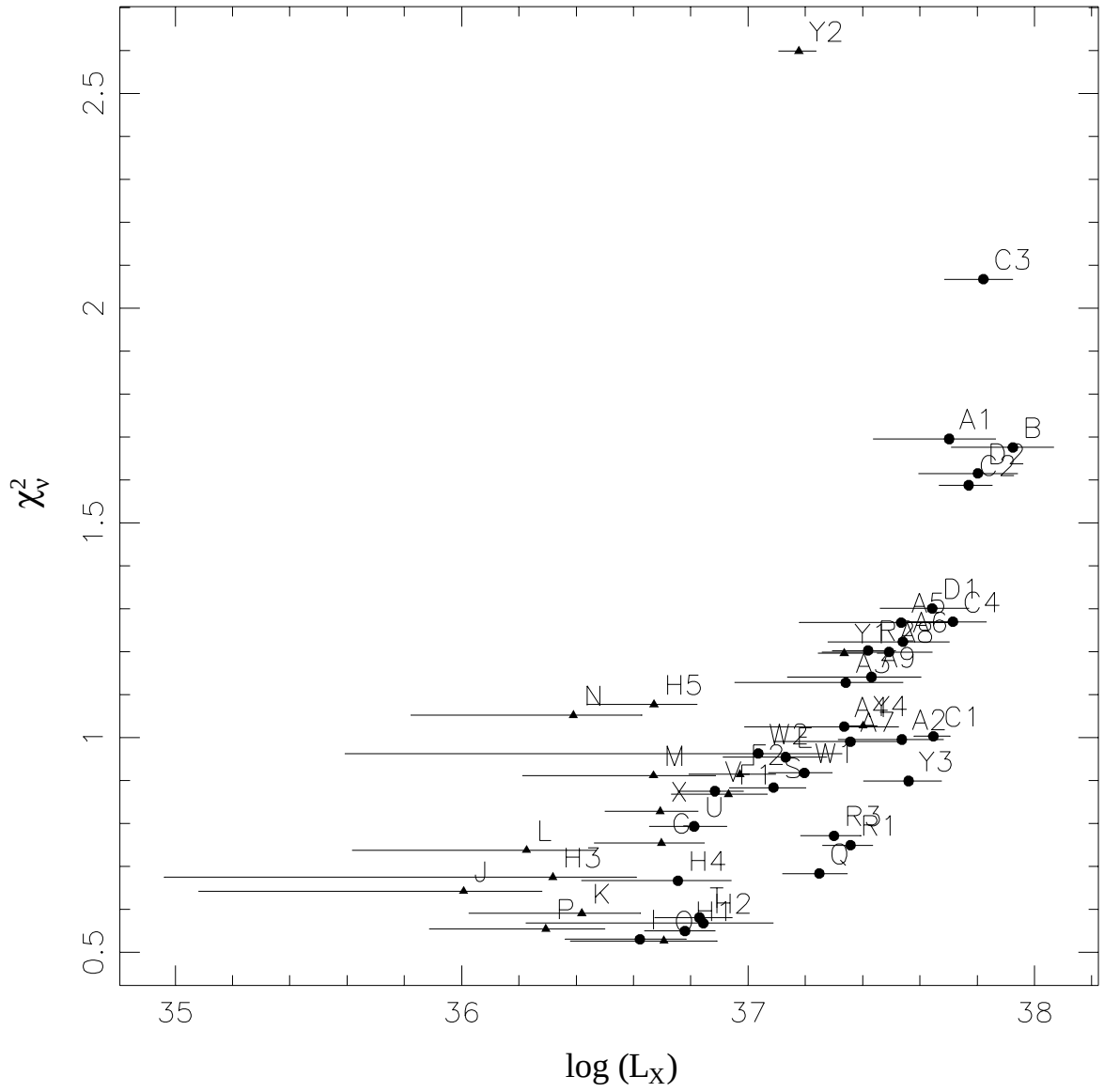

Fig. 3.— Reduced-χ^2 for fits to *RXTE* spectra from GX 1+4 using an analytic Comptonization continuum component (`compTT` in XSPEC) as a function of 2–60 keV flux (assuming a source distance of 10 kpc). Spectral range for fitting is typically 2.5–35 keV. Circles indicate those fits where all the spectral parameters are free to vary, while for observations marked by triangles at least one parameter (usually T_e) is fixed in order to obtain error limits on the other parameters. The markers are labelled with the letter corresponding to the observation, in some cases also with a number where the observation has been divided into separate intervals for spectral analysis. Errorbars show 90 per cent limits on flux calculated from the variance in the phase-averaged countrate over each observation (see Figure 1).

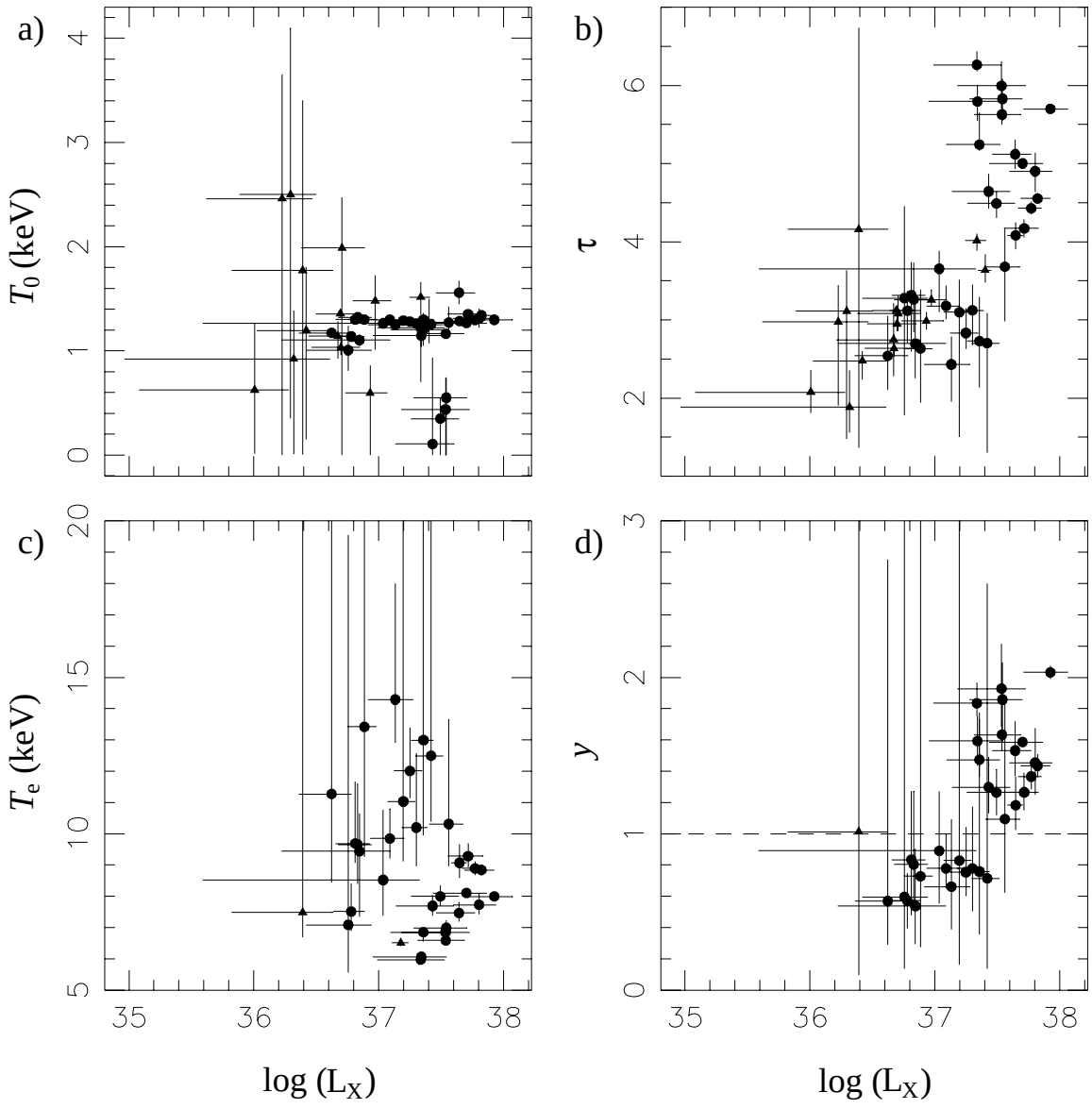

Fig. 4.— Fit values for the Comptonization continuum component ('compTT' in XSPEC) parameters for spectral fits to *RXTE* observations of GX 1+4 versus unabsorbed 2–60 keV flux (assuming a source distance of 10 kpc). a) Source spectrum temperature T_0; b) optical depth for scattering τ; c) plasma temperature T_e; and d) Compton y-parameter (calculated from the fitted τ and T_e values). Errorbars show 90 per cent confidence limits. Other details are as for Figure 3.

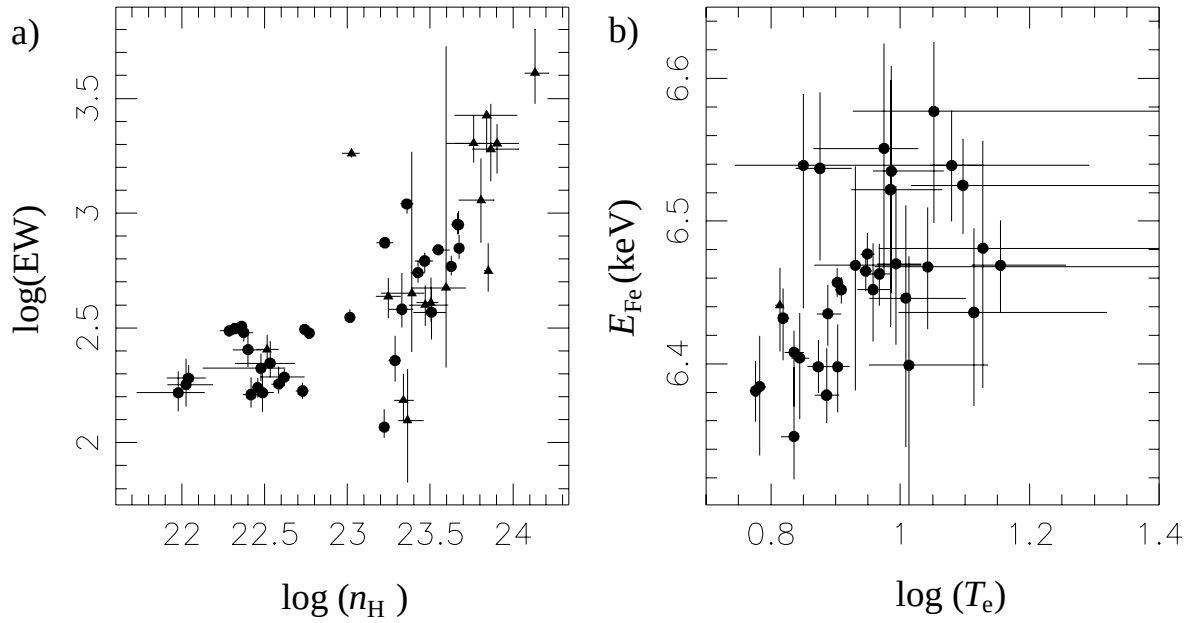

Fig. 5.— a) Iron line equivalent width (EW) plotted as a function of absorption column density $n_{\rm H}$. b) Iron line gaussian centre energy plotted as a function of the plasma temperature $T_{\rm e}$. Errorbars show 90 per cent confidence limits. Other details are as for Figure 3.

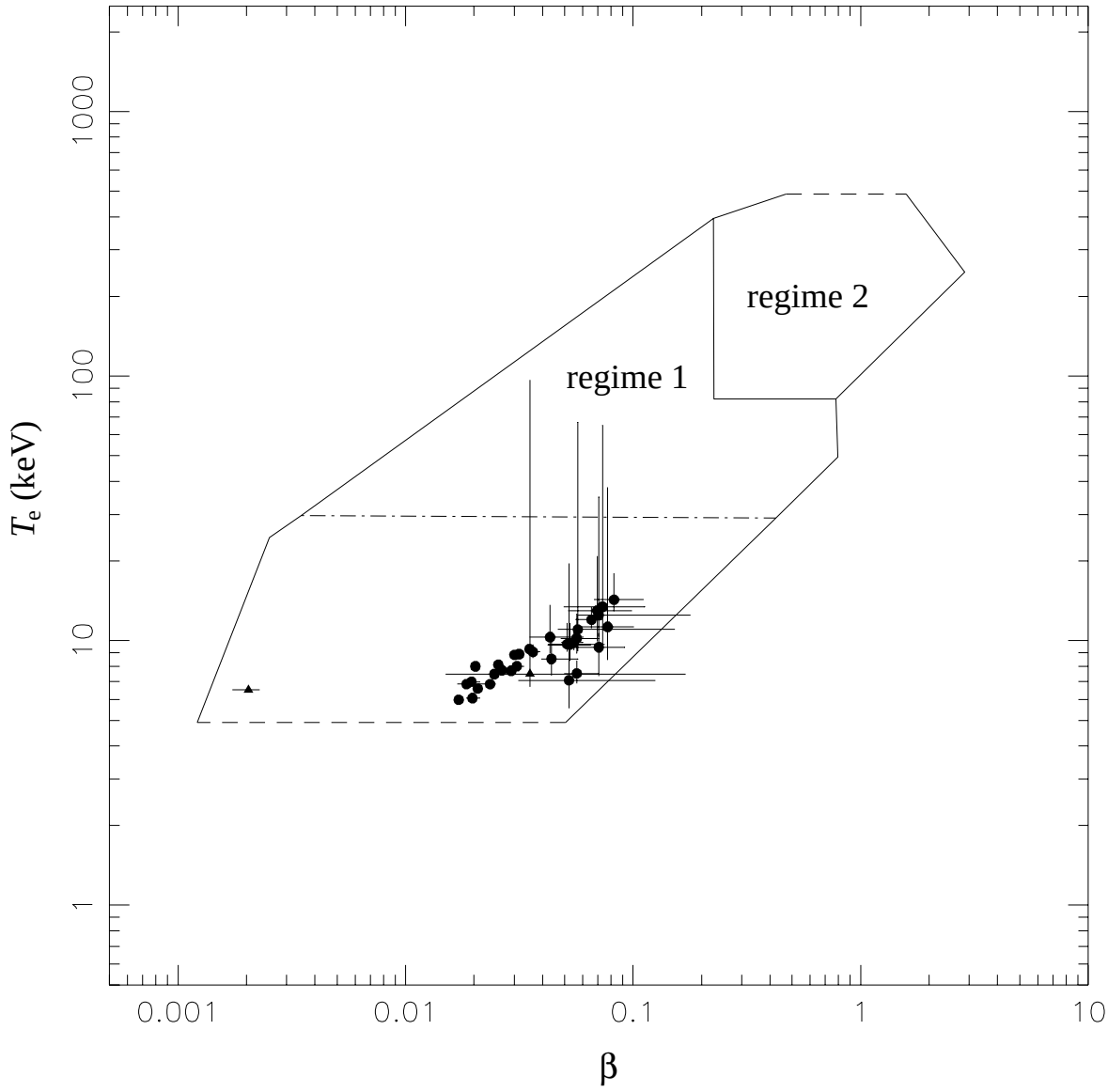

Fig. 6.— Scattering plasma temperature T_e versus Titarchuk β-parameter appropriate for disc geometries (equation 2). The enclosed regions are those plotted in Figure 7 of Hua & Titarchuk (1995), and delineate the range of parameters over which the analytical model of Titarchuk (1994) is consistent with equivalent Monte Carlo calculations. Errorbars show 90 per cent confidence limits.